Milk protein-shelled gold nanoparticles with gastrointestinally active absorption for aurotherapy to brain tumor

Hyung Shik Kim [a], Seung Jae Lee [a], Dong Yun Lee [a,b,*]

[a] Department of Bioengineering, College of Engineering, and BK FOUR Biopharmaceutical Innovation Leader for Education and Research Group, Hanyang University, Seoul, 04763, Republic of Korea
[b] Institute of Nano Science and Technology, Hanyang University, Seoul, 04763, Republic of Korea

ABSTRACT

Orally absorbable gold nanoparticles (AuNP) having cancer ablation therapy is strongly demanded to treat glioblastoma multiforme (GBM) for patients with its highest incidence rate. Here, we develop a milk protein lactoferrin-conjugated AuNP for its oral absorption and targeting to the GBM through the interaction between lactoferrin (Lf) and lactoferrin receptor (LfR) that is highly expressed in the intestine, blood-brain barrier and GBM. For stability and long circulation of AuNP, glutathione and polyethylene glycol (PEG) is introduced, which is called to Lf-PEG-AuNP. When Lf-PEG-AuNP are orally administered to orthotopic GBM-bearing mice, 11-fold and 8-fold higher concentrations of AuNP are measured in bloodstreams and GBM in the brain, respectively, compared with unconjugated-AuNP. Therefore, orally administered Lf-PEG-AuNP exhibit an outstanding temperature rise in GBM by irradiating laser and significantly reduce tumor volume. Collectively, we suggest that the Lf-PEG-AuNP can fundamentally target GBM in the brain through oral absorption, and that its efficient photothermal therapy is possible.

1. Introduction

Glioblastoma multiforme (GBM) is the most common primary grade 4 brain tumor and a severe central nervous system disease. GBM has a high incidence rate in the elderly, and is characterized by a poor clinical prognosis, high invasiveness, a high mortality rate, and frequent recurrences [1]. Recent therapeutic approaches of GBM include focal radiotherapy and adjuvant chemotherapy after surgical resection [2]. However, due to the delicate anatomical structure of the brain and the surrounding blood-brain barrier (BBB), conventional invasive surgical therapy and drug injections with short half-lives rarely achieve successful treatment results [3]. The development of alternative approaches to effectively treat GBM is one of the most pressing challenges [4].

Gold nanoparticles (AuNP) have been studied in tumor therapy. Especially, AuNP are used in photothermal therapy (PTT) treatment of GBM due to the physical nature of the surface plasmon resonance (SPR) effect that generates heat by irradiating near-infrared (NIR) light [5–7]. AuNP with a size range of 5–100 nm have a mechanism that enables to pass through the BBB due to vascular leakage as a brain tumor progresses [8,9]. As a result, AuNP can accumulate within the tumor through the enhanced permeability and retention (EPR) effect, allowing them to discriminate between normal brain and tumor tissue [10,11].

However, the EPR effect alone is not sufficient when attempting to systemic delivery of AuNPs to GBM. Improvement of blood stability and half-life must be considered, and sufficient delivery becomes possible only when a selective targeting method for GBM is additionally applied to AuNP [12]. Effective GBM treatment through PTT will be conquered once methods that can effectively deliver AuNP to GBM are developed.

Among the various drug delivery routes, the oral route is drawing the most attention due to its advantages, such as sustained and controllable delivery, ease of administration, and patient compliance [13–16]. In addition, the large surface area of the gastrointestinal (GI) tract (>300 m^2), which is lined with viscous mucous membranes, retains the drug for a long time and serves for subsequent absorption [17]. Orally administered drugs are absorbed in four types of pathways: receptor-mediated transcellular, carrier-mediated transcellular, paracellular, and facilitated transport [18]. However the acidic environment of the GI tract during the oral absorption process cause agglomeration of AuNP [19]. Agglomerated AuNP are not able to penetrate the intestinal epithelium [20] and consequently reduce the oral absorption efficiency of AuNP [21].

To overcome the limitations for low bioavailability of AuNP to target GBM through oral administration, we targeted the lactoferrin receptor (LfR) commonly expressed in the GI tract [22], BBB and GBM [23].

Fig. 1. Mechanism of action and synthesis process of Lf-PEG-AuNP enabling PTT therapy in GBM tissue in the brain after oral absorption. (a) Schematic illustration for oral absorption and GBM targeting of Lf-PEG-AuNP through LfR pathway of the small intestine, the BBB barrier, and GBM cells. (b) Synthetic procedure of Lf-PEG-AuNP via a PEG linker between Lf protein and AuNP.

Therefore, we conjugated lactoferrin (Lf) on the surface of glutathione (GSH)-coated AuNPs (5 nm in diameter) with a polyethylene glycol (PEG) linker; that was Lf-PEG-AuNP. GSH and PEG increased the stability of Lf-PEG-AuNP in the GI tract, and Lf served to enhance oral absorption and the targeting of GBM through LfR-mediated transport. Thus, a sufficient amount of Lf-PEG-AuNP were accumulated to GBM and it enable GBM to be treated with PTT. Selective destruction of GBM could be achieved by targeted Lf-PEG-AuNP which were irradiated by PTT laser (Fig. 1a).

2. Experimental section/methods

2.1. Materials

Gold (III) chloride trihydrate (HAuCl₄), glutathione (GSH), human lactoferrin (hLf), sodium hydroxide (NaOH), sodium borohydride (NaBH₄), 100-kDa and 10-kDa MWCO dialysis tubing cellulose membrane, 1-ethyl-3-(3-dimethylaminopropyl) carbodiimide (EDC), n-hydroxysuccinimide (NHS), osmium tetroxide (OsO₄), pepsin, Spurr low-viscosity embedding kit, paraformaldehyde, cresyl violet-acetate,

acetic acid and sodium acetate were purchased from Sigma-Aldrich, MO, USA. bifunctional poly(ethylene glycols) (SH-PEG-COOH) were purchased from Quanta BioDesign, Plain City, USA). JEM-301 HR-TEM grids were purchased from Nanolab Technologies, NY, USA. InstantBlue™ was purchased from Expedeon, UK. BCA protein assay kit was purchased from Pierce Biotechnology, Rockford, IL, USA. Transwell insert was purchased from Corning, Inc., Corning, New York, USA. Cell cytotoxicity assay EZ-Cytox was purchased from DoGenBio, Seoul, Korea. 3% isoflurane was purchased from HanaPharm, Seoul, Korea. in 150 mL of distilled water and a buffer solution containing 0.1 M. DeadEnd Fluorometric Terminal deoxynucleotidyl transferase dUTP nick end labeling (TUNEL) System kit was purchased from Promega, USA.

2.2. Experimental cell lines and animals

All experiments were carried out using HUVECs (LONZA, NJ, USA), the Caco-2 cell line (Korean Cell Line Bank, Seoul, Korea), and a human glioblastoma (GBM) cell line (U87MG; Korean Cell Line Bank, Seoul, Korea). HUVECs (passage numbers 4 to 6) were cultured using endothelial growth medium (EGM-2 bullet kit; LONZA, NJ, USA), Caco-2 cells were cultured using Dulbecco's Modified Eagle's Medium (DMEM; GenDEPOT, TX, USA) containing 10% fetal bovine serum (FBS; GenDEPOT), 1% penicillin-streptomycin and 0.2% MEM in standard culture conditions at 37 °C and 5% CO_2. GBM cells were cultured using DMEM containing 10% FBS and 1% penicillin-streptomycin in standard culture conditions at 37 °C and 5% CO_2.

2.3. Animal purchase and study approval

Male BALB/c nude mice of seven-week-old were purchased from Nara-Bio Company, Seoul, Korea. Mice were controlled in Specific Pathogen-Free (SPF) condition in accordance with the provisions of the Institutional Animal Care and Use Committee (IACUC) at Hanyang University. Feed was given once a day and an automated watering system was used. The experimental protocol was approved by IACUC (No. 2017-0034A) and conformed to the guidelines for the Care and Use of Laboratory Animals.

2.4. Synthesis of lactoferrin-conjugated AuNP (Lf-PEG-AuNP)

HAuCl$_4$ (11.1×10^{-3} M), GSH (37.8×10^{-3} M), and NaOH (178×10^{-3} M) were dissolved in 20 mL of methanol/water solution (1.3:1 v/v). Then, this solution (20 mL) was diluted to a final Au^{3+} concentration 0.48×10^{-3} M with the addition of methanol (104 mL) and water (294 mL). The Au^{3+} was reduced with the addition of 4 mL of NaBH$_4$ (0.25 M). The reduction of Au was allowed to proceed for 24 h at 100 °C with constant stirring. AuNP were precipitated with the addition of 68 mM of NaCl (68×10^{-3} M) in methanol (200 mL) and followed by centrifugation (3200 rpm for 5 min). Precipitated nanoparticles were reconstituted in water. The wavelength-dependent molar extinction coefficient (ε) of 45,000 cm^{-1}/M at 532-nm wavelength for the AuNP solution was calculated with UV–visible spectroscopy according to the Beer-Lambert law:

$$A(\lambda) = \log_{10} \frac{I_0}{I} = \varepsilon cl,$$

where $A(\lambda)$ is the measured wavelength-dependent absorbance, I_0 is the incident light intensity, I is the transmitted light intensity, c is the concentration of the substrate, and l is the pathlength of the quartz cuvette (0.1 cm). The diameters of the AuNP (about 5 nm) were measured by high-resolution TEM (HR-TEM; JEM-2100, JEOL, Matsudo, Japan). On the other hand, Lf was conjugated with carboxyl group of bifunctional poly(ethylene glycols) (SH-PEG-COOH). Briefly, a solution of 1-ethyl-3-(3-dimethylaminopropyl) carbodiimide (EDC; 250×10^{-3} M) and of n-

hydroxysuccinimide (NHS; 500×10^{-3} M) were dissolved in PBS containing SH-PEG-COOH (12.5×10^{-3} M) during constant stirring. After approximately 15 min, Lf (0.125×10^{-3} M) was further added in the solution and reacted at 4 °C with constant stirring for 24 h. The resultant Lf-PEG conjugates were collected by dialysis with a 10 kDa-pore membrane at 4 °C, and then it was freeze-dried. After that, this Lf-PEG was mixed with SH-PEG-COOH in PBS at 4 °C with constant stirring (SH-PEG-COOH: SH-PEG-Lf = 4:1 ratio, and solution of AuNP (40×10^{-6} M) was further treated for 24 h to conjugate the thiol group of PEG and Lf-PEG onto the surface of AuNP. The resultant Lf-PEG-AuNP conjugates were collected by dialysis with 100 kDa-pore membrane at 4 °C.

2.5. Characterization of Lf-PEG-AuNP

The synthesized AuNP and Lf-PEG-AuNP were analyzed with HR-TEM. The subsequent TEM images were analyzed by Image-J software (US National Institutes of Health, Bethesda, Maryland, USA) to determine the size distribution of the AuNP. Samples of Lf-PEG-AuNP were dissolved in distilled water (DW) and were characterized using a 500 MHz NMR Avance-500 (Bruker, Germany). To identify the size-dependent SPR effects, both AuNP and Lf-PEG-AuNP were measured by a UV–visible spectrophotometer (NanoDrop 2000; Thermo Scientific, Wilmington, USA). For SDS-PAGE, sample were prepared by mixing Lf-PEG-AuNP/free Lf ratio of 1:1.4 (v/v) sample. The gel was stained by InstantBlue™, was destained by a destaining solution (40% methanol and 10% glacial acetic acid), and then the band on the gel was analyzed with Image-J software. On the other hand, BCA protein assay kit was used to calculate the binding ratio between Lf and PEG. The heating profiles of the AuNP and Lf-PEG-AuNP were confirmed using a thermal camera (FLIR C2, Oregon, Wilsonville, USA). An NIR diode laser (LRS-0532 DPSS Laser System; 532 nm; Laser glow Part Number: R5310B1FL, Toronto, ON, Canada) was applied to vials containing of AuNP and Lf-PEG-AuNP (gold equivalent concentration of 10×10^{-6} M) concentration, respectively, for 240 s.

2.6. Stability of Lf-PEG-AuNP in GI tract biomimicking conditions

AuNP and Lf-PEG-AuNP (50×10^{-6} M) were applied at each pH 2 and 5 for 0, 1, 3, 6, 9 and 12 h, which mimicked the gastric and small intestine environment. During this time, the absorbances and temperature of the AuNP and Lf-PEG-AuNP were measured with a UV–visible spectrophotometer and a thermal camera with irradiation from an NIR diode laser. Proteolytic degradation test using pepsin enzyme was used to investigate the stability of Lf-PEG-AuNP from protease as a digestive enzyme. Each Lf and Lf-PEG samples was dissolved in 1 mL of HCl (10×10^{-3} M), and then were mixed with pepsin solution (60 μL, 40 ng mL^{-1}) with ratio of 1:1 (v/v), respectively. Each sample was incubated in the CO_2 incubator with 37 °C for 1, 10, 20, 30, 60, 120 or 240 min. Next, each reacted sample (120 μL) was added with a $4 \times$ SDS sample solution (30 μL), and then the mixture was immersed in a water bath (50 °C for 5 min). Finally, the reacted sample was analyzed with gel electrophoresis with (10% polyacrylamide). The band on the gel was stained with Coomassie Brilliant Blue R-250 (0.1%). After destaining with a solution (40% methanol and 10% glacial acetic acid), the bands were quantified by Image-J software.

2.7. Permeability of Lf-PEG-AuNP through Caco-2 cell monolayer

For cell viability assays, HUVECs and Caco-2 cells were seeded in 96-well plates at a density of 5×10^3 cells in each well and were incubated for 24 h in the CO_2 incubator. Then, AuNP or Lf-PEG-AuNP (10×10^{-6} M gold equivalent concentration) was treated for 24 h. After washing with PBS buffer, they were treated with culture medium containing EZ-Cytox (10%) at 37 °C and 5% CO_2 for 4 h. The absorbance of medium was measured with a micro-well plate reader (450-nm wavelength). To evaluate the permeability of AuNP or Lf-PEG-AuNP through the Caco-2

cell monolayer, the Caco-2 cells were seeded in the transwell insert (6.5-mm diameter and 0.4-μm pore size) with seeding density of 2×10^4 cells in each insert. Then, they were cultured for 3 weeks in the CO_2 incubator. To check the tight junction between them, the transepithelial electrical resistance (TEER) was measured using a voltmeter (EVOM2; World Precision Instruments, Sarasota, USA). The TEER value > 3700 Ω cm^2 was used for the assay. Caco-2 cells were treated with AuNP or Lf-PEG-AuNP (10 μM gold equivalent concentration). For competitive binding, free Lf (5×10^{-6} M) was pretreated for 2 h and then further treated with Lf-PEG-AuNP (10×10^{-6} M gold equivalent concentration). During treatment, TEER values were measured at each time. To confirm the penetration of AuNP and Lf-PEG-AuNP through the Caco-2 cell monolayer, they were observed by using TEM.

2.8. TEM procedure for detection of AuNP and Lf-PEG-AuNP

Sorensen's phosphate buffer, which is composed of solutions A and B (A is 0.2°M $Na_2HPO_4 \cdot 2H_2O$ and B is 0.2°M $NaH_2PO_4 \cdot H_2O$), was added for 10 min to rinse off the fixative. Next, 1% osmium tetroxide (OsO_4) was added to stain the Caco-2 cell monolayer or tissue membrane for 1 h. Then the samples were washed with Sorensen's phosphate buffer for 10 min to eliminate the remaining OsO_4. Dehydration of the samples was performed with different concentration of ethanol as follows: 30% for 10 min; 50% for 10 min; 70% for 10 min; 90% for 10 min; and finally, 100% for 20 min with 3 times. The formation of epoxy resin block with a low viscosity embedded media Spurr's Kit method was applied to all of the samples. The epoxy resin specimens were cut into 80-nm-thick sections using an ultramicrotome (EM UC7, Germany), and the obtained sections were air-dried for at least 1 h. Copper grids were mounted with 2% uranyl acetate for 20 min, briefly washed with distilled water, and mounted onto lead citrate (0.4%) for staining for 10 min. The section placed on the grid was observed using an 80 kV TEM.

2.9. In vitro photothermal therapeutic efficacy of Lf-PEG-AuNP on GBM cells

To confirm the uptake of AuNP or Lf-PEG-AuNP, the GBM cells with seeding density of 5×10^4 cells for each well were treated with AuNPs or Lf-PEG-AuNPs (10×10^{-6} M M gold equivalent concentration) for 18 h. After washing three times with PBS, then cells were detached with trypsin/EDTA, centrifuged (1000 rpm for 3 min) and analyzed with TEM. On the other hand, to evaluate whether GBM cells were damaged, they were treated with Lf-PEG-AuNP, AuNP, and Lf for 24 h. Then the viability of GBM cells were measured with EZ-Cytox kit. To measure the photothermal effect of the uptaken Lf-PEG-AuNP, the GBM cells were treated with Lf-PEG-AuNP, AuNP, and Lf for 18 h and then were irradiated with an NIR diode laser (5 min). The viability of them was measured with EZ-Cytox kit. On the other hand, to evaluate whether the Lf-PEG-AuNP could be stably maintained during cell division, the GBM cells were treated with Lf-PEG-AuNP, AuNP, or Lf for 18 h. After that, the cells were washed for elimination of remaining drugs and then serially cultured for 18 h without drugs. After 18 h of additional incubation, the GBM cells were irradiated with an NIR diode laser (5 min). Then the viability of GBM cells were measured with EZ-Cytox kit.

2.10. In vivo orthotopic GBM-bearing mice modeling

To prepare the orthotopic GBM-bearing mice, GBM cells (U87MG cell) were intracranially injected into 7-week-old male nude mice. Briefly, male nude mice were anesthetized with isoflurane (3%) and fixed by ear bar in a stereotaxic instrument (Stoelting Co., IL, USA). Once each mouse was anesthetized, the scalp at the surgical position was removed and a small hole positioned at 2 mm right lateral and 2 mm posterior from the bregma was drilled under sterile conditions. After that, 8 μL PBS having 1×10^6 U87MG cells were loaded into a 26-G Hamilton syringe (Hamilton Company, NV, USA), and then the syringe

was placed on the stereotaxic apparatus. After the needle of the syringe was positioned at 3 mm depth, cells were injected with a 1 μL min^{-1} injection rate and followed by 3 min of waiting time for prevention of overflow. After injection, the hole was sealed with bone wax and the scalp was closed with suturing. After this procedure, the mice were breed for 3 weeks until the injected cells reached the appropriate size of GBM tissue.

2.11. Oral absorption Lf-PEG-AuNP through the small intestine in the GBM-bearing mice

GBM-bearing BALB/c mice were fasted for 6 h, and then 100 μl of AuNPs (11 mg kg^{-1}) and Lf-PEG-AuNPs (60 mg kg^{-1}) were orally administered with an oral gavage, respectively. Mice were sacrificed 2.5 h after oral administration. The small intestine including the duodenum, jejunum and ileum were separated and fixed with paraformaldehyde (4%) for TEM. On the other hand, to measure the absolute amount of gold absorbed in the mice model, the exact weights of samples were measured in a borosilicate glass tube. Next, 800 μl of nitric acid (70%) was added to each glass tube and samples were heated at 60 °C in a hot water bath for 3 h. Thereafter, HCl (37%) was added to each glass tube, and samples were heated in the same conditions. The digested blood or tissues were transferred into 50 mL tubes and adjusted to nitric acid (2%) and HCl (0.5%) with distilled water. The solutions were filtered using pore-size filters (0.22 μm) and analyzed by the inductively coupled plasma-mass spectrometry (ICP-MS). The Au concentration in the sample was quantify by using a standard curve of Au (0.0001–0.05 μg mL^{-1}) with 0.0005 μg mL^{-1} of detection limit. The gold concentration in each sample was determined from the mean of six replicate measurements. On the other hand, to quantify the content of AuNP in the bloodstream, the blood samples were collected via retro-orbital plexus bleeding techniques at each time after oral administration of AuNPs and Lf-PEG-AuNPs, and were analyzed by ICP-MS. To evaluate GBM targeting efficacy in the brain, the brain in the mice was excised for ICP-MS and TEM analysis 24 h after oral administration of AuNP or Lf-PEG-AuNP. Also, the content of AuNP in other organs such as kidney, spleen, heart, lung, and liver were measured by ICP-MS analysis.

2.12. In vivo photothermal therapeutic efficacy of Lf-PEG-AuNP on GBM tissue in the brain

To evaluate the photothermal effect of AuNP and Lf-PEG-AuNP targeted to the GBM tissue in the brain, the temperature change by PTT laser irradiation were measured. 100 μl of AuNPs (11 mg kg^{-1}) and Lf-PEG-AuNPs (60 mg kg^{-1}) were orally administered with an oral gavage, respectively. As a control group, PBS (vehicle) was orally administered. After 24 h of oral administration, an NIR diode laser (4 W/cm^2) was irradiated to the GBM-bearing head region or the left torso in the mice for 180 s. The thermal camera (FLIR C2, FLIR) were used to measure the temperature change in the laser irradiation region. After 3 repetitive treatments for 7 days, GBM-bearing brains were excised, sectioned, and stained. For Nissl staining, the brain slides were stained with a stain solution that prepared by dissolving cresyl violet-acetate (0.2 g) in DW (150 mL) and a buffer solution containing acetic acid (0.1 M) and sodium acetate (0.1 M). H&E staining and the TUNEL System kit were used to detect the apoptosis in the brain slides following the manufacturer's instruction. On the other hand, for the RES organ toxicology study, 100 μl of AuNPs (11 mg kg^{-1}) and Lf-PEG-AuNPs (60 mg kg^{-1}) were orally administered with an oral gavage 5 times at intervals of 2 days., respectively. After 5 times oral administration for 10 days, the kidney, liver, lung and spleen were excised for the histology analysis. All data were calculated using the region of interest function of Image-J software.
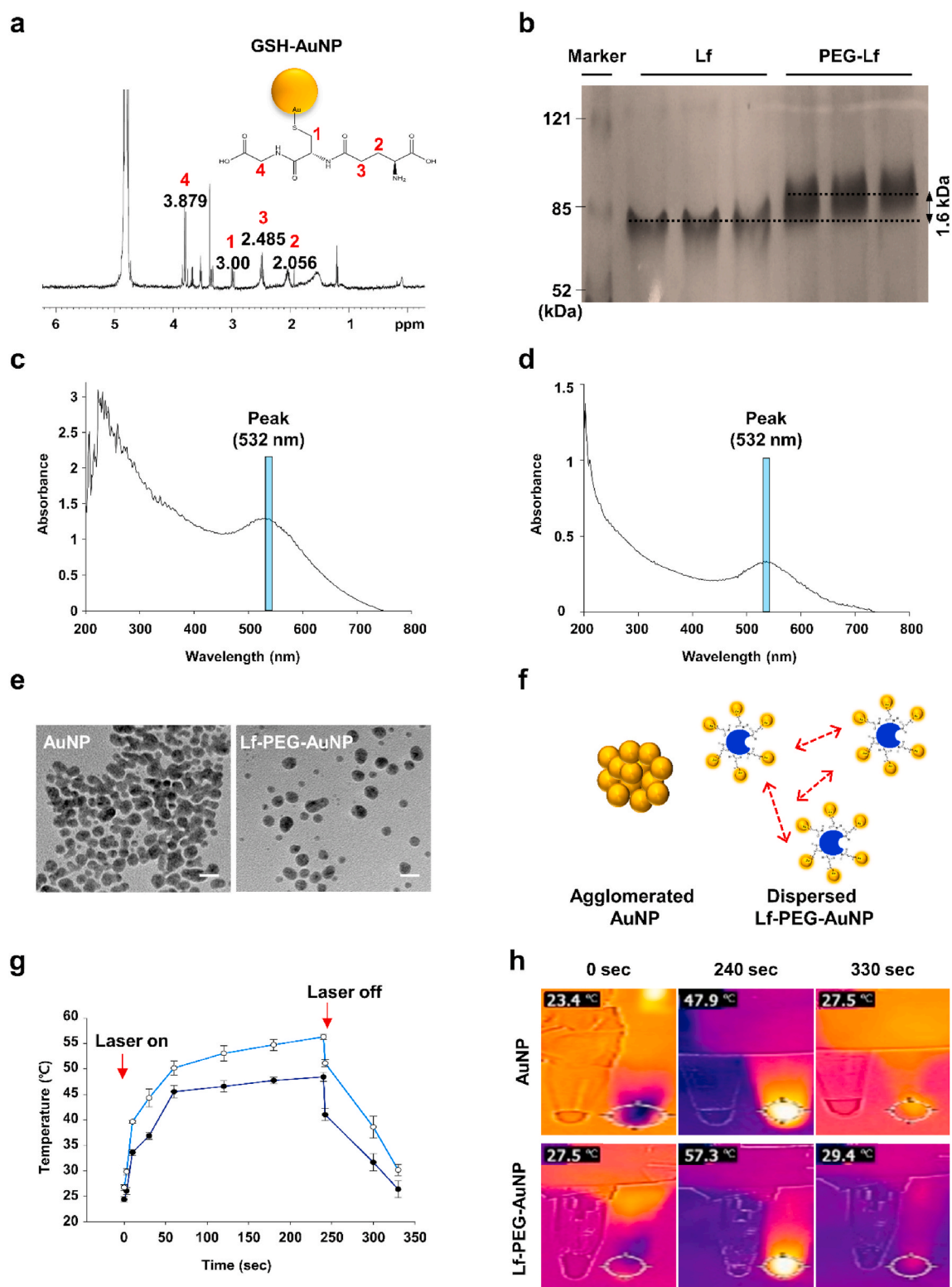
Fig. 2. Characterization of Lf-PEG-AuNP. (a) NMR spectra of GSH-AuNP. (b) SDS-PAGE of Lf and PEG-Lf. (c) UV–Vis absorption spectra of AuNP with a peak at 532 nm wavelength. (d) UV–Vis absorption spectra Lf-PEG-AuNP with a peak at 532 nm wavelength. (e) TEM images of AuNP and Lf-PEG-AuNP. Scale bar: 10 nm. (f) Schematic diagram of AuNP agglomeration and Lf-PEG-AuNP dispersion by the repulsive effect of PEG. (g) Temperature change of AuNP itself and Lf-PEG-AuNP during PTT laser irradiation. Data were expressed as means ± SEM (n = 4). (h) Thermal images of AuNP itself and Lf-PEG-AuNP during PTT laser irradiation at each time.
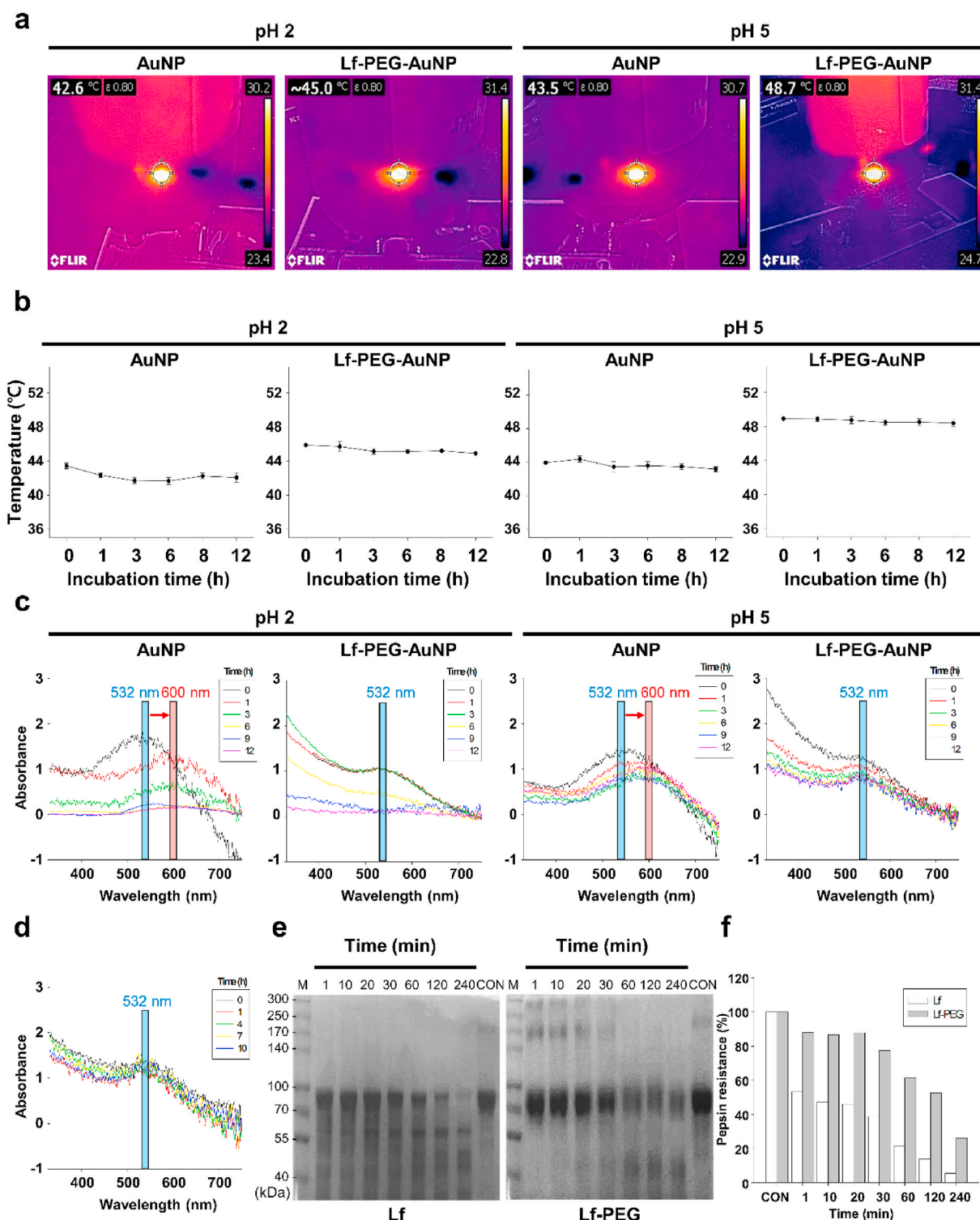
Fig. 3. The stability of Lf-PEG-AuNP according to exposure to the gastrointestinal tract environments. (a) Thermal images of AuNP and Lf-PEG-AuNP by PTT laser irradiation after exposure at pH 2 and pH 5 for 12 h. (b) Thermal images of AuNP and Lf-PEG-AuNP by PTT laser irradiation after exposure at pH 2 and pH 5 at each incubation time. Data were expressed as means ± SEM (n = 5). (c) UV–Vis absorption spectrum of AuNP and Lf-PEG-AuNP after exposure at pH 2 and pH 5 for 12 h. Peak shift from 532-nm to 600-nm wavelength. (d) UV–Vis absorption spectrum of Lf-PEG-AuNP after exposure at pH 2 for 2 h and serial exposure at pH 5 for 8 h. (e) Proteolytic degradation of Lf and Lf-PEG during incubation time with pepsin enzyme. (f) The resistance of Lf and Lf-PEG from pepsin enzyme through the densitometrically analysis of the band at Fig. 3e.

2.13. Statistical analysis

All data were expressed as mean ± standard error of the mean (SEM). Statistically significant differences were evaluated using Student's *t*-tests or one-way analysis of variance (ANOVA) (Systat Software Inc., San Jose, CA, USA). *P*-values less than 0.05 were considered statistically significant.
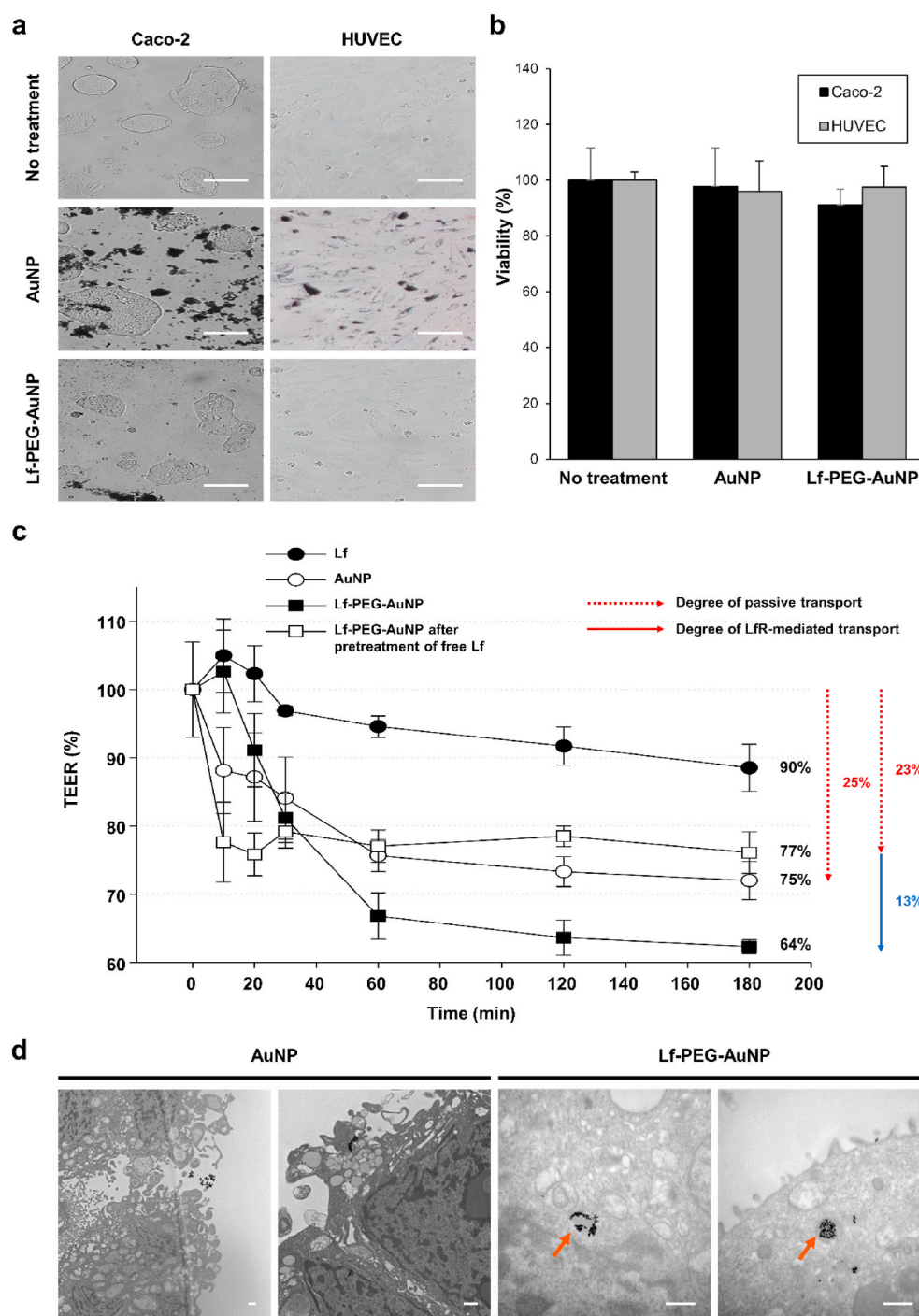
Fig. 4. Toxicity and permeability of Lf-PEG-AuNP through the intestinal Caco-2 cell monolayer and endothelial cells. (a) Morphology of the intestinal Caco-2 cells and human umbilical vein endothelial cells (HUVECs) after treatment of AuNP or Lf-PEG-AuNP for 24 h. Magnification: × 100. Scale bar: 100 μm. (b) The viability of Caco-2 cells and HUVECs after treatment of AuNP or Lf-PEG-AuNP for 24 h. Data were expressed as means ± SEM (n = 6). (c) TEER values through Caco-2 cell monolayer after treatment of each group for 24 h. Data were expressed as means ± SEM (n = 3). (d) TEM images of the Caco-2 cell monolayer after AuNP and Lf-PEG-AuNP. Orange arrows: Lf-PEG-AuNP through LfR endocytosis. Scale bar: 500 nm. (For interpretation of the references to color in this figure legend, the reader is referred to the Web version of this article.)

3. Results and discussion

3.1. Synthesis and characterization of Lf-PEG-AuNP

To increase the low absorption efficiency of AuNP in the GI tract, we synthesized Lf-PEG-AuNP (Fig. 1b). The 3.0 ppm peak in the ^{1}H nuclear magnetic resonance (NMR) spectrum of the GSH-AuNP indicated that the multichemical environment at the AuNP interface of the proton attached to the C site (1) around the –SH group of GSH. The resonance expansion of protons at 2.056 (2), 2.485 (3) and 3.879 (4) ppm indicated that GSH was coated on the AuNP surface (Fig. 2a). [24–26] The molecular weight (MW) of the synthesized GSH-AuNP is 63.6 kDa, and it was calculated using the correlation between the measured molar

concentration and the mass of the lyophilized GSH-AuNP (Fig. S1).

The successful synthesis of PEGylated-Lf (Lf-PEG) could be assumed based on the sodium dodecyl sulfate polyacrylamide gel electrophoresis (SDS-PAGE) results, showing a 1.6 kDa rise in the band above 80 kDa, which is the MW of native Lf (Fig. 2b). In addition, the BCA assay results showed that the 50 PEG molecules were bound to one Lf protein molecule in the Lf-PEG conjugate (Fig. S2a). The Lf-PEG formed a disulfide bond on the GSH-AuNP surface via the PEG with a thiol group. As a result, Lf-PEG-AuNP nanoconjugates were synthesized such that approximately 19.7 GSH-AuNP were bound to one Lf-PEG (Fig. S2b). Using UV–Vis spectrophotometry, we observed peaks in the same 532-nm wavelength band in both AuNP and Lf-PEG-AuNP, verifying that the unique SPR effect of AuNP was maintained in the Lf-PEG-AuNP

produced through various synthetic processes (Fig. 2c and d). The plasmon resonance peaks of AuNP relied heavily on the nanoparticle size. Smaller AuNP particles had peaks near 530 nm, while larger AuNP particles had peaks shifted toward longer wavelengths. Transmission electron microscopy (TEM) images show that the actual size of the AuNP and Lf-PEG-AuNP particles was 5 nm in diameter (Fig. 2e). In the TEM images, AuNPs were strongly agglomerated, whereas Lf-PEG-AuNPs were well dispersed [27] (Fig. 2f). The colloidal stability of Lf-PEG-AuNPs was attributed to the unconjugated PEG molecules (approximately 60% of totally conjugated PEG molecules) on the Lf protein. Additionally, the nanoparticles with a size of 30 nm or less are

generally transferred to not only the cytoplasm but also the cell nucleus [28]. Therefore, Lf-PEG-AuNP, which maintains a size of 5 nm by through steric stabilization, could be efficiently absorbed by target cells.

To verify the SPR efficiency of AuNP and Lf-PEG-AuNP, the temperature changes of them were measured for up to 330 s under PTT laser irradiation (4 W/cm^2 intensity). During 240 s of PTT laser irradiation, the temperature of AuNP and Lf-PEG-AuNP was maintained at an elevated state of 48–57 °C, and quickly returned to room temperature within a few seconds after stopping laser irradiation. In addition, Lf-PEG-AuNP showed the enhanced heating efficiency with a difference of about 10 °C at the maximum temperature, compared to the AuNP
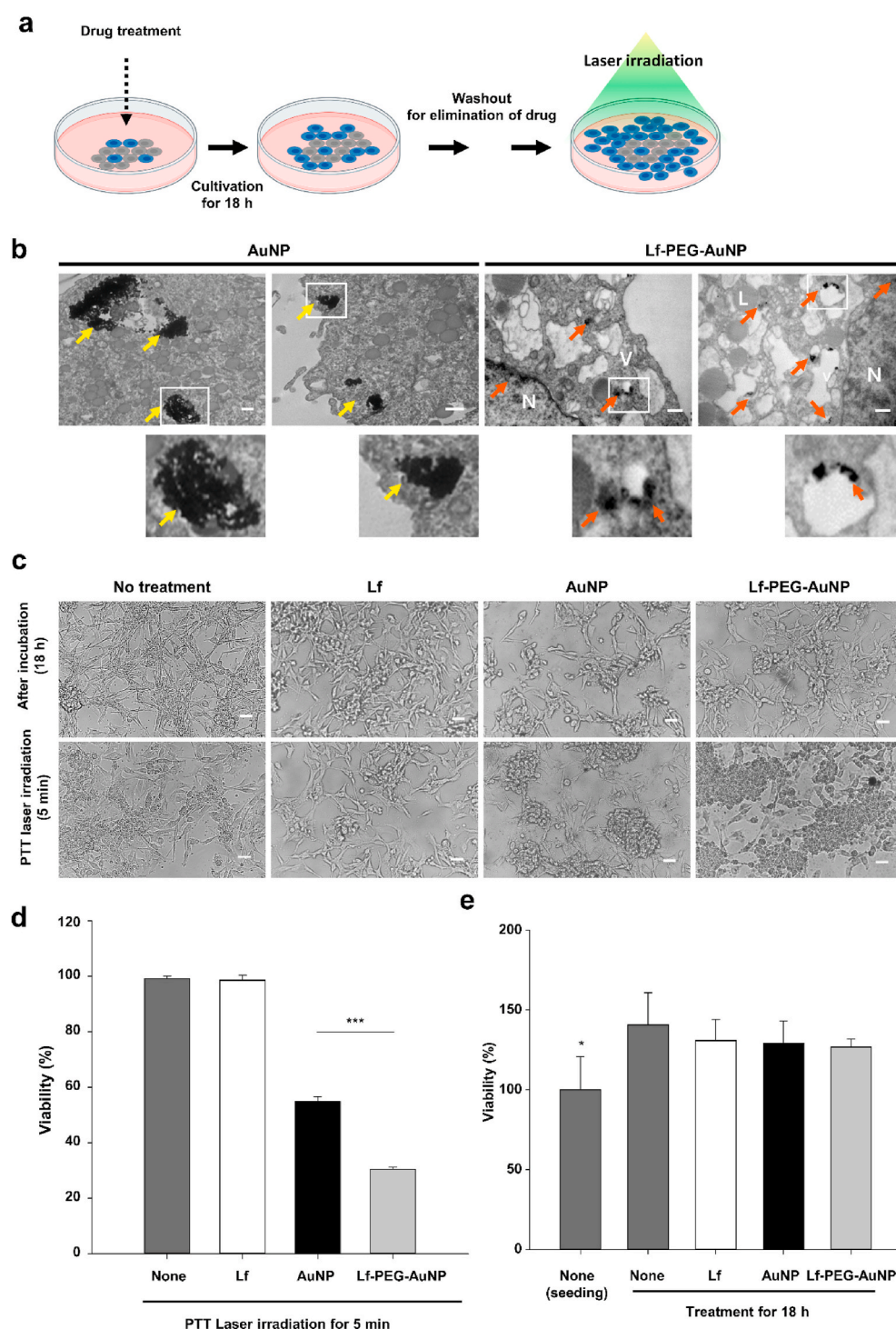

Fig. 5. Intracellular accumulation and therapeutic effect of Lf-PEG-AuNP to GBM cells after PTT laser irradiation. (a) A schematic illustration for experimental strategy of PTT effect of Lf-PEG-AuNP accumulated in the GBM cell. (b) TEM images of GBM cells treated with AuNP and Lf-PEG-AuNP for 18 h. Insert image: magnified image of square area. Yellow arrow: aggregated AuNP in the GBM cells. Orange arrows: Lf-PEG-AuNP through LfR endocytosis. L: lysosome, V: vesicles in the cytoplasm, N: nucleus. Scale bar: 500 nm. (c) Morphology of GBM cells after PTT laser irradiation for 5 min. Magnification: × 200. Scale bar: 250 μm. (d) The viability of GBM cells after PTT laser irradiation for 5 min. Data were expressed as means ± SEM (n = 5). ***P < 0.001. (d) The viability of GBM cells after 18 h treatment of each group. Data were expressed as means ± SEM (n = 5). *P < 0.05. (For interpretation of the references to color in this figure legend, the reader is referred to the Web version of this article.)

itself (Fig. 2g and h). Accordance to several literatures, cell destruction increased linearly in PTT laser intensity range of 1.5–4.7 W/cm^2 [29]. Based on our findings, the laser intensity of 4 W/cm^2 could be sufficient to generate PTT therapeutic effect. Therefore, we continuously used 4 W/cm^2 intensity of PTT laser to the following experiment without optimization. Also, the enhanced heating capacity of Lf-PEG-AuNP might be the result of preventing agglomeration between AuNP due to the repulsion effect of Lf-PEG. Furthermore, considering the criterion of *in vivo* PTT agent that have to generate heat above 45 °C [30], Lf-PEG-AuNP could meet this criterion and could be sufficiently applied as a PTT agent in further experiments.

3.2. Stability of Lf-PEG-AuNP in a gastrointestinal-mimicking environment

For targeted oral delivery to GBM using AuNP, firstly Lf-PEG-AuNP should need to be absorbed in the gastrointestinal (GI) tract. To evaluate the stability of both AuNP and Lf-PEG-AuNP during oral absorption procedure, we mimicked the pH environments of the gastric and intestinal systems. Thus, the changes in colloidal stability of AuNP and Lf-PEG-AuNP in the acidic pH 2 and pH 5 were measured at different time period by variation in heating capacity through laser irradiation. For 12 h, AuNP and Lf-PEG-AuNP at pH 2 were maintained at 42.6 ± 1.2 °C and 45.0 ± 1.1 °C, respectively. In the result of pH 5, they were 43.5 ± 1.5 °C and 48.7 ± 1.4 °C, respectively (Fig. 3a and b, Fig. S3). The temperature variation over time was ~1 °C in all groups, but the heat generated by Lf-PEG-AuNP was significantly higher than that of AuNP itself under both pH 2 and 5. For further validation, the 532-nm plasmon peaks of the AuNP and Lf-PEG-AuNP were monitored with UV–visible spectrophotometry. In the case of the AuNP group at pH 2 and pH 5, the extent of the absorbance peak was significantly reduced after 1 h of exposure. In addition, the peak was shifted from 532-nm to 600-nm due to the agglomeration of AuNP. On the other hand, since the Lf-PEG-AuNP were dispersed without agglomeration between particles, the initial absorbance value was maintained at pH 2 and pH 5 without peak shift (Fig. 3c). These results demonstrated that Lf-PEG-AuNP relatively well maintains colloidal stability in an acidic environment. On the other hand, administered orally drugs remain typically in the gastric for 2 h and in the intestine for 8 h, respectively [19]. Therefore, to more specifically simulate the oral absorption procedure of Lf-PEG-AuNP, it was serially exposed to pH 2 for 2 h and then pH 5 for an additional 8 h. Lf-PEG-AuNP still showed stability without peak shift and absorbance reduction at the 532-nm wavelength band (Fig. 3d). Based on these findings, it demonstrated the suitability of Lf-PEG-AuNP as an oral formulation.

When Lf-PEG-AuNP was orally administered, Lf hydrolysis by gastric pepsin enzyme could act as a barrier in the absorption process of Lf-PEG-AuNP through the LfR. The pepsin proteolysis test was determined by quantifying the remaining band at the position of 80 kDa molecular weight of intact Lf. As a result, the Lf-PEG showed higher pepsin resistance compared to the Lf itself (Fig. 3e and f). The PEGylation of Lf increased resistance to hydrolysis because it inhibited enzymatic adsorption and protected Lf from proteolysis [31]. The results of proteolysis resistance of Lf-PEG and the enhanced colloidal stability of Lf-PEG-AuNP under acidic conditions indicated that Lf-PEG-AuNP would be stably absorbed from the GI tract [32].

3.3. In vitro Lf-PEG-AuNP capable oral absorption by LfR at the small intestine cell membrane

Next, we evaluated whether AuNP and Lf-PEG-AuNP could pass through the small intestine. Frist of all, we confirmed no toxicity of
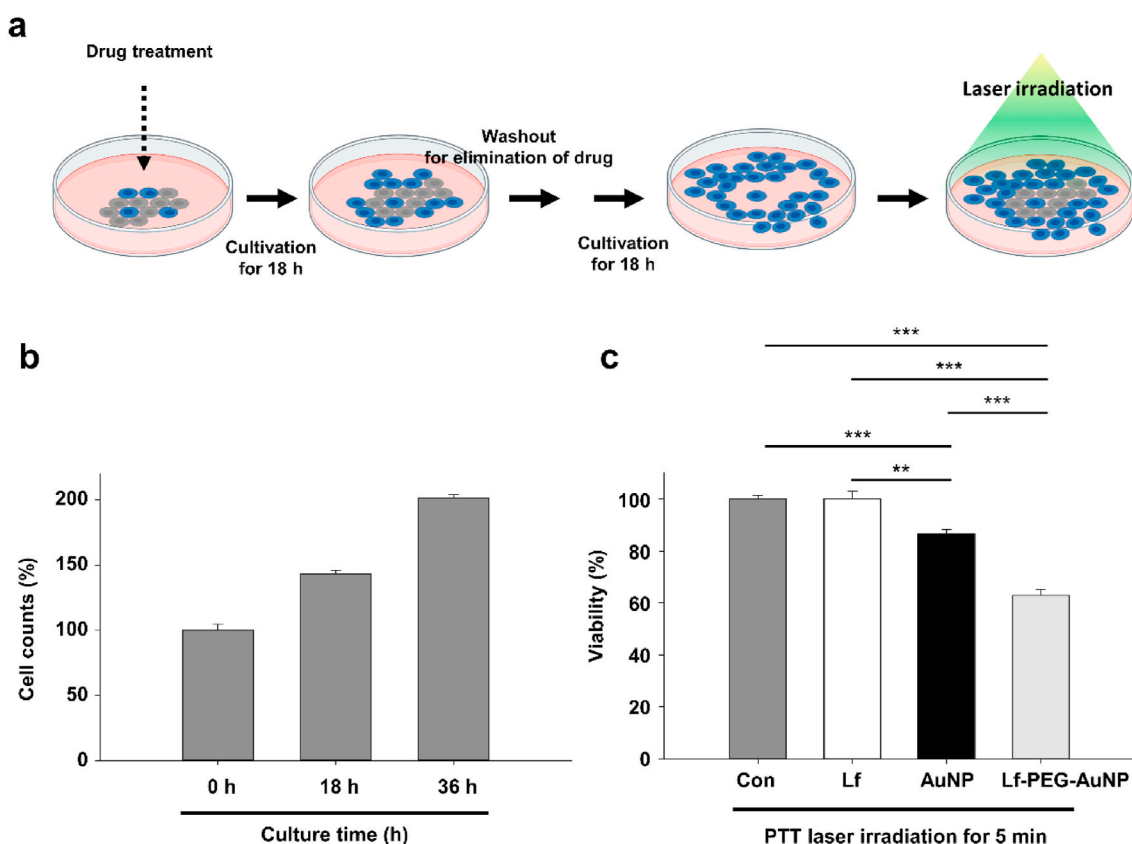

Fig. 6. PTT effect of stably accumulated Lf-PEG-AuNP during GBM cell division. (a) A schematic illustration for experimental strategy of PTT effect of stably accumulated Lf-PEG-AuNP during GBM cell division. (b) Proliferation of GBM cells by cell division for 36 h cultivation. (c) The viability of GBM cells accumulated with AuNP and Lf-PEG-AuNP after PTT laser irradiation for 5 min. Data were expressed as means ± SEM (n = 5). **P < 0.01. ***P < 0.001.
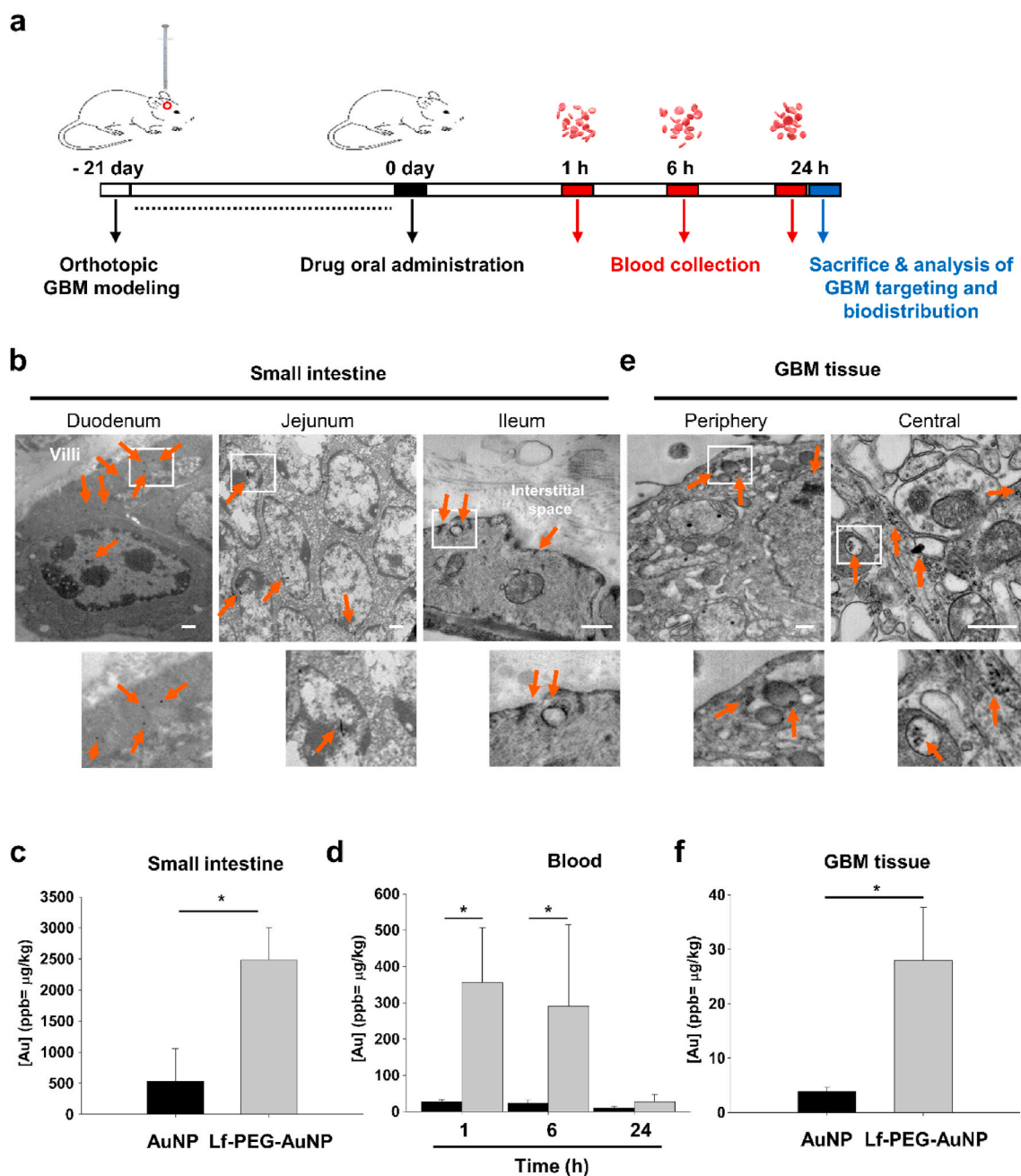
Fig. 7. Oral absorption and GBM targeting of Lf-PEG-AuNP in orthotopic GBM-bearing mice *in vivo*. (a) Schematic illustration of orthotopic GBM modeling and sampling of blood and tissues. (b) TEM images of the small intestine at 2.5 h after oral administration of Lf-PEG-AuNP. Insert image: magnified image of square area. Orange arrows: Lf-PEG-AuNP. Scale bar: 500 nm. (c) Quantification of AuNP (black bar) and Lf-PEG-AuNP (gray bar) in the intestine at 24 h after oral administration. Data were expressed as means ± SEM (n = 5). *P < 0.01. (d) Quantification of AuNP (black bar) and Lf-PEG-AuNP (gray bar) in blood samples at each time after oral administration. Data were expressed as means ± SEM (n = 5). **P < 0.01. (e) TEM images of periphery and central of GBM tissue in the brain at 24 h after oral administration of Lf-PEG-AuNP. Insert image: magnified image of square area. Orange arrows: Lf-PEG-AuNP. Scale bar: 500 nm. (f) Quantification of AuNP (black bar) and Lf-PEG-AuNP (gray bar) in the small intestine and the GBM tissue in the brain 24 h after oral administration. Data were expressed as means ± SEM (n = 5). *P < 0.05. (For interpretation of the references to color in this figure legend, the reader is referred to the Web version of this article.)

AuNP and Lf-PEG-AuNP on the morphology and viability of Caco-2 cells and human umbilical vein endothelial cells (HUVECs) during 24 h incubation. (Fig. 4a and b). Then, the Caco-2 cell permeability was performed to determine whether the permeation of Lf-PEG-AuNP was increased by LfR in the small intestinal epithelium. Several intestinal epithelial cells, including Caco-2 cell, are known to express the LfR abundantly [33]. The transepithelial electrical resistance (TEER) assay is reliable and easy to implement permeability test [34]. Therefore, it is a standard model for the prognosis of oral drug absorption and for mechanisms of drug transport [35–38]. The TEER value decreases as

drug transmittance in the Caco-2 cell monolayer, indicating the permeability of the drug. To this end, we confirmed that the Caco-2 cells became the monolayer to prevent non-specific passage of the drugs by forming tight junctions between cells (Fig. S4). When Lf itself, AuNP, and Lf-PEG-AuNP were treated to the Caco-2 cell monolayer, the TEER values at each group decreased over time to approximately 90.1 ± 3.4, 75.0 ± 2.8 and 64.2 ± 1.2%, respectively (Fig. 4c). It is expected that the enhanced permeability of Lf-PEG-AuNP (~36% permeability) was due to the LfR-mediated transport. In the Bio TEM images, the presence of the intracellular Lf-PEG-AuNP in the Caco-2 cell monolayer

elucidated the LfR-mediated transcytosis (Fig. 4d). However, AuNP itself could be slightly penetrated through the Caco-2 cell monolayer via passive transport through the tight junctions between the cells. On the other hand, to clearly verify the passive transport of Lf-PEG-AuNP by excluding the LfR-mediated transcytosis, the LfRs on the Caco-2 cell monolayer were fully occupied with free Lf in advance and then Lf-PEG-AuNP was further treated (Fig. S5). As a result, the TEER value of the Lf-PEG-AuNP with pretreatment of free Lf was ~77%, which was almost the same as that of the AuNP (Fig. 4c). This result suggested that 23% of Lf-PEG-AuNP also passively transport through the tight junction between cells of the Caco-2 cell monolayer, as did AuNP. Furthermore, the 13% difference between the Lf-PEG-AuNP with pretreatment of free Lf (~23% permeability) and the Lf-PEG-AuNP alone (~36% permeability) could be interpreted as the effect of LfR-mediated transport. Collectively, these results demonstrated that Lf-PEG-AuNP could effectively penetrate through the intestinal epithelium via active and passive transport simultaneously. On the other hand, we did not yet study the mechanism using the blood-brain carrier (BBB) chip that has been recently reported [39]. Therefore, we will investigate the penetration mechanism of Lf-PEG-AuNP using the BBB chip system.

3.4. Excellent PTT effect by stably accumulating Lf-PEG-AuNP in GBM cell in vitro

Next, we evaluated the PTT effect of Lf-PEG-AuNP in GBM cell *in vitro*. To this end, we firstly checked its internalization into the GBM cells. Lf-PEG-AuNP was observed in the endosome vesicles through endocytosis and also detected in the nucleus (Fig. 5a). However, AuNP itself was detected as cytoplasmic aggregation although they were also internalized into the GBM cells. Therefore, it is possible that Lf-PEG-AuNP could strongly affect the GBM cells due to its complete distribution in the cytoplasm and nucleus. In fact, the internalized AuNP and Lf-PEG-AuNP significantly affected the viability of GBM cells after PTT laser irradiation for 5 min (Fig. 5b). But Lf-PEG-AuNP could much strongly damage the viability of GBM cells when compared to the AuNP (Fig. 5c). To evaluate whether the reduced viability of GBM cells was not related to the existence of AuNP or Lf-PEG-AuNP, the number of GBM cells were counted after treatment for 18 h when is typical doubling time of GBM proliferation [40]. There was no inhibition effect of Lf, AuNP, and Lf-PEG-AuNP itself for 18 h cultivation (Fig. 5d). This result showed that AuNP and Lf-PEG-AuNP do not affect cell proliferation in the absence of PTT laser irradiation. Collectively, we found that the internalized AuNP and Lf-PEG-AuNP could reduce the viability of GBM cells and that Lf-PEG-AuNP dispersed in the GBM cell could have much effective phototoxicity with high sensitivity to PTT laser irradiation. From these experiments, we wondered whether the internalized AuNP and Lf-PEG-AuNP were stably existed without leakage during GBM cell division. To confirm that, we first cultured GBM cells with AuNP or Lf-PEG-AuNP for 18 h and then further cultured them without AuNP and Lf-PEG-AuNP for 18 h after washout (Fig. 6a). The number of proliferated GBM cells was continuously increased during cultivation (Fig. 6b). After that, the cultured GBM cells were directly applied with PTT laser irradiation for 5 min. As a result, the number of GBM cells treated with AuNP and Lf-PEG-AuNP was significantly reduced (Fig. 6c). In addition, Lf-PEG-AuNP still strongly affect the viability of GBM although GBM cells were cultured for twice doubling times. However, the effect of AuNP itself was significantly reduced after additional cultivation for 18 h when compared to the effect of AuNP after 18 h treatment (see Fig. 5c), which might be attributed to the AuNP aggregation in the cytosol. Collectively, these results demonstrated that Lf-PEG-AuNP was effectively well-retained in the first-accumulated parental cells during cell division.

Table 1
Biodistribution of orally administered AuNP and Lf-PEG-AuNP. Gold accumulation of organs after 24 h of administration of AuNP and Lf-PEG-AuNP that measured by ICP-MS. Data were expressed as means ± SEM (n = 4).

	Kidney	Spleen	Heart	Lung	Liver
AuNP [Au] (ppb = μg/kg)	64.0 ± 31.0	85.3 ± 54.9	61.9 ± 47.3	49.4 ± 46.1	22.5 ± 11.7
Lf-PEG-AuNP [Au] (ppb = μg/kg)	65.8 ± 35.2	66.9 ± 22.8	185.9 ± 88.7[a]	108.7 ± 76.6[a]	22.0 ± 14.1

[a] $P < 0.01$ versus AuNP itself group.

3.5. Enhanced oral absorption and GBM tissue targeting of Lf-PEG-AuNP in orthotopic GBM-bearing mice

To evaluate whether Lf-PEG-AuNP could be orally absorbed and targeted to GBM tissue in the brain, GBM-bearing mice were established 3 weeks before oral administration of Lf-PEG-AuNP (Fig. 7a). The blood samples and tissues were harvested at each time after oral administration of Lf-PEG-AuNP. A large amount of Lf-PEG-AuNP were detected at the whole area of small intestine including duodenum, jejunum, and ileum at 2.5 h after oral administration (Fig. 7b; arrow). The amount of AuNP itself and Lf-PEG-AuNP in the small intestine were 531.3 ± 456.5 and 2484.3 ± 522.8 μg kg^{-1}, respectively (Fig. 7c), suggesting that Lf-PEG-AuNP could be significantly absorbed 5-fold more than AuNP itself. There were several literatures for oral absorption of AuNP by using various molecular weights of PEG polymer [21,41,42]. Lower molecular weight of PEG polymer (<1 kDa) could improve the oral absorption of AuNP in the intestine, which might be related to the repulsive effect of PEG polymer at the colloidal stability of AuNP in the aqueous solution and AuNP repulsion on the surface of the intestine. In our study, lower molecular weight of PEG polymer (232 Da) was used as a linker between Lf and AuNP. Interestingly, PEG polymer could protect the Lf from the proteolytic degradation by digestive enzyme (see Fig. 3), thereby enhancing the active transport of Lf-PEG-AuNP via LfR pathway. Subsequently, Lf-PEG-AuNP were highly absorbed into the bloodstream through the capillaries of small intestine (Fig. 7d). The amount of AuNP itself and Lf-PEG-AuNP in the bloodstream were 26.3 ± 15.3 and 355.2 ± 370.8 μg kg^{-1}, respectively, at 1 h after oral administration. Then there were almost disappeared in the bloodstream at 24 after oral administration. Afterward, the Lf-PEG-AuNP and AuNP were systemically circulated through bloodstream. Fortunately, Lf-PEG-AuNP could target to the periphery and central area of GBM tissue in the brain (Fig. 7e, arrow). The targeted amount of AuNP itself and Lf-PEG-AuNP to the GBM tissue were 3.8 ± 0.8 and 27.9 ± 9.8 μg kg^{-1}, respectively, at 24 h after oral administration (Fig. 7f). Lf-PEG-AuNP were significantly targeted 8-fold more than AuNP itself. Compared to targeting effect of AuNP itself and Lf-PEG-AuNP, they were intravenously injected into the bloodstream. The amount of AuNP itself and Lf-PEG-AuNP in the GBM tissue in the brain were 142.0 ± 21.2 and 230.0 ± 35.5 μg kg^{-1}, respectively, at 24 h after intravenous injection (Fig. S6). Based on these finding, we found that the conjugated Lf could significantly improve the AuNP targeting to the GBM tissue. On the other hand, we observed lower accumulation of AuNP itself in the GBM tissue. The reason might be attributed to the BBB destruction and EPR effect, which are commonly caused by abnormal angiogenesis and tumor pressure in GBM lesions [43–46].

3.6. Biodistribution of orally administered Lf-PEG-AuNP to other organs

In general, the large amount of systemically injected AuNP tend to be eliminated from the blood by the reticuloendothelial system (RES) and accumulated in several organs such as the kidney, spleen, and liver [47–51]. Especially, liver and spleen are considered two main organs for the biodistribution and metabolism of AuNP. Moreover, the distribution of AuNP to those organs depends on their size, and particles with a size
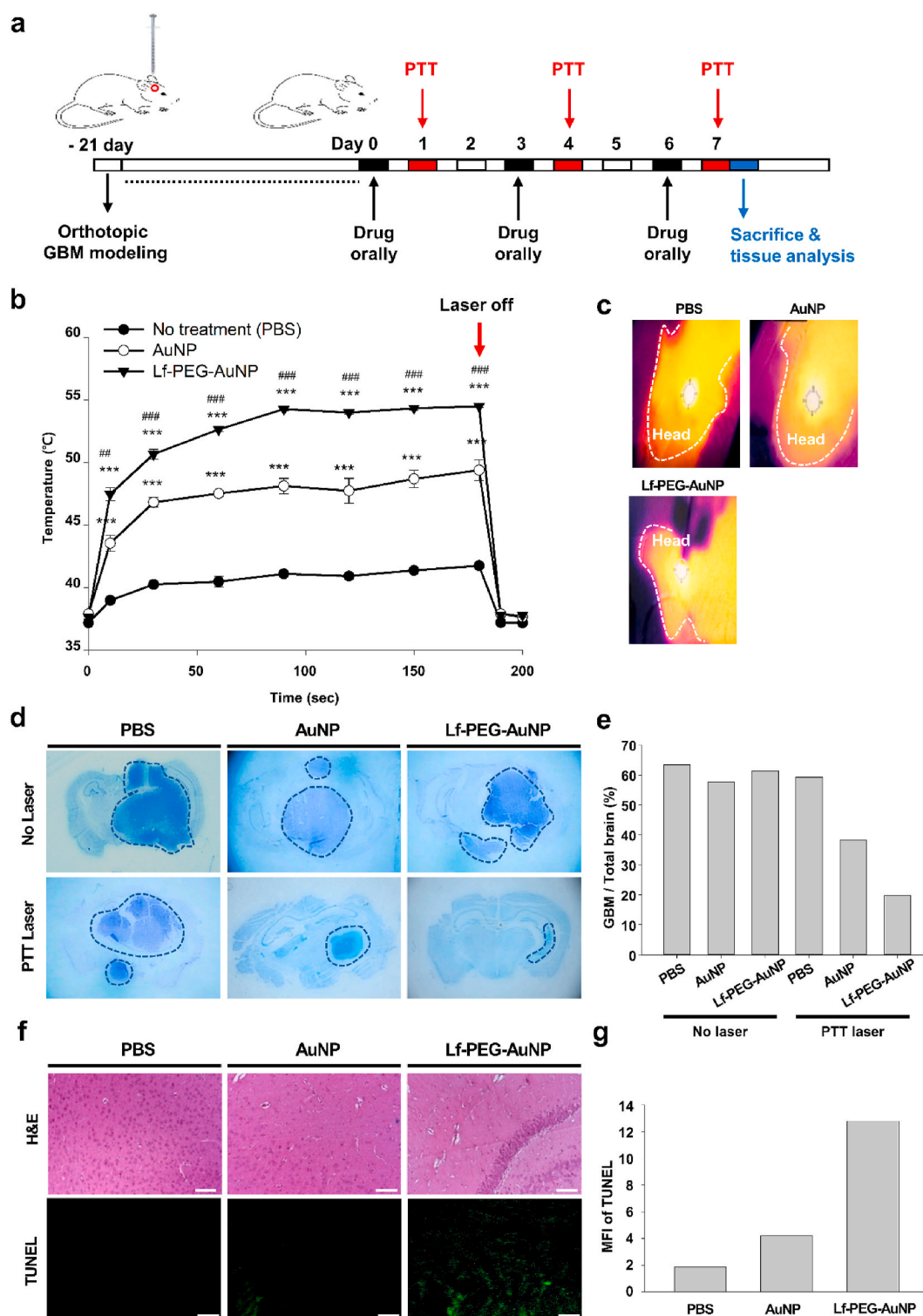
Fig. 8. Therapeutic effect in orthotopic GBM-bearing mice after repetitive oral administration and PTT laser irradiation. (a) Schematic illustration of the experimental strategy for repetitive oral administration and PTT laser irradiation. The GBM tissues in the brain were harvested and analyzed 7 days after repetitive treatment. (b) Temperature measurements of the head of GBM-bearing mice during PTT laser irradiation for 180 s. Data were expressed as the mean $\pm$ SEM (n = 5). ***$P < 0.001$ versus No treatment (PBS vehicle) group. $^{\#\#}P < 0.01$ versus AuNP group. $^{\#\#\#}P < 0.001$ versus AuNP group. (c) Thermal images of mice heads (dashed line) during PTT laser irradiation. (d) Nissl dye-stained images of GBM-bearing brain sections after 3 times repetitive oral administration and PTT laser irradiation. Dashed line: GBM tissue area. Magnification: $\times$ 40. (e) Proportion of GBM in the brain from the Nissl results. (f) H&E stain and TUNEL immunostain of GBM tissues. Green color: TUNEL-positive apoptotic cells. Sale bar: 50 μm. (g) Mean fluorescence intensity (MFI) of TUNEL results. (For interpretation of the references to color in this figure legend, the reader is referred to the Web version of this article.)

of 5–15 nm have a wider distribution than larger ones [52,53]. Therefore, we measured the biodistribution of orally administered Lf-PEG-AuNP and AuNP. Despite of low absorption, the amount of AuNP was accumulated similarly to that of Lf-PEG-AuNP at kidney, spleen, and liver (Table 1). Interestingly, the amount of Lf-PEG-AuNP was significantly accumulated at the heart and lung compared to that of AuNP itself. Recent studies have shown that the LfR-like intelectin is prominently expressed in pericardium mesothelial cells, intestinal epithelial cells, and lung epithelial cells [54–57]. Therefore, the orally absorbed Lf-PEG-AuNP could be slightly accumulated at the heart and lung tissue. On the other hand, although Lf-PEG-AuNPs were administered orally five times in succession, there was no damage of the kidney, liver, lung, or spleen tissue based on the histological analysis (Fig. S7). In addition, there was no change in spleen tissue size when monitoring strong immunogenicity, even though Lf-PEG-AuNP was repeatedly administered orally. Furthermore, there was no adverse behavior among the experimental animals in terms of food intake or weight loss during oral administration of Lf-PEG-AuNP. Therefore, Lf-PEG-AuNP can be reliably used to target GBM tissue in the brain without damage to other tissues.

3.7. Therapeutic effect of orally administered Lf-PEG-AuNP in orthotopic GBM-bearing mice

To investigate PTT efficacy of orally administered Lf-PEG-AuNP *in vivo*, AuNP itself and Lf-PEG-AuNP were orally administered to orthotopic GBM-bearing mice and then PTT laser was irradiated to the head of the mice 24 h after oral administration, repetitively (Fig. 8a). When Lf-PEG-AuNP-administered mice were irradiated with PTT laser, the temperature at the head of mice was dramatically increased, while AuNP-administered mice showed significantly lower temperature at the head of mice (Fig. 8b and c; Supplementary Movie S1~S3). As control group, PBS vehicle-administered mice showed very lower temperature at the head of mice. At 180 s after PTT laser irradiation, the temperature of the head of mice administered with PBS, AuNP, and Lf-PEG-AuNP was 41.7 ± 0.1, 49.4 ± 0.8, and 54.5 ± 0.1 °C, respectively. On the other hand, when the left torso of AuNP- and Lf-PEG-AuNP-administered mice were irradiated with PTT laser, the temperature of the torso area was 45.9 ± 1.1, and 41.8 ± 0.1 °C, respectively (Fig. S8 and Supplementary Movie S4 and S5). Based on these finding, we found the Lf-PEG-AuNP had higher targeting effect to the GBM tissue in the brain with lower non-specific distribution to other organs.

Supplementary data related to this article can be found at https://doi.org/10.1016/j.bioactmat.2021.06.026.

To confirm PTT effect of orally administered Lf-PEG-AuNP, the GBM-bearing brain tissues were harvested, sectioned and stained for visualization of GBM tissue in the brain. Without PTT laser irradiation, the area of Nissl dye-positive GBM tissue in the brain was very similar to all groups (Fig. 8d and e). After 3 times repetitively oral administration of AuNP itself and PTT laser irradiation, the area of Nissl dye-positive GBM tissue in the brain was attenuated. Interestingly, when Lf-PEG-AuNP was repetitively administered and irradiated with PTT laser, the area of Nissl dye-positive GBM tissue in the brain was almost cleared. To confirm the damage of the GBM tissue in the brain, H&E stain and TUNEL immunostain were carried out (Fig. 8f and g). In the case of Lf-PEG-AuNP treatment, the nuclei of the GBM cells were significantly attenuated, which was attributed to the apoptosis of GBM cells via the PTT effect of Lf-PEG-AuNP. Therefore, Lf-PEG-AuNP can be used to cure GBM tissue in the brain via PTT laser irradiation. On the other hand, it is well known that GBM is characterized by its invasiveness with high mortality and that the survival rate following diagnosis is 12–15 months. Since the survival rate is still the most important aspect of treatment, we therefore evaluate the long-term survival rate of GBM-bearing mice after oral delivery of Lf-PEG-AuNP with PTT laser irradiation.

4. Conclusion

In this study, we developed Lf-PEG-AuNP as a PTT therapeutic agent for GBM therapy. It was orally absorbed with resistance of proteolytic digestion and its half-life in the blood was improved due to its colloidal stability. The conjugated lactoferrin protein can prevent aggregation of Lf-PEG-AuNP, thereby showing a stronger PTT effect. Additionally, it can enhance the oral absorption of Lf-PEG-AuNP via interaction with Lf receptors (LfR) in the small intestine. Therefore, orally absorbed Lf-PEG-AuNPs significantly targeted GBM tissue in the brain via the interaction with LfR on the GBM tissue, thereby providing therapeutic effects with PTT laser irradiation. Thus, milk protein Lf shell can be used a platform system for gastrointestinal active absorption and targeting GBM for aurotherapy of the brain. However, the stability of Lf protein should be further elucidated during oral absorption to improve the targeting efficacy of Lf-PEG-AuNPs to GBM. Prospectively, when Lf-PEG-AuNP delivery is used with focal radiotherapy and adjuvant chemotherapy after surgical resection, it can be used as a combinational therapeutic agent for synergistic treatment of glioblastoma.

CRediT authorship contribution statement

Hyung Shik Kim: Conceptualization, Methodology, Investigation, Validation, Formal analysis, Writing – original draft, Writing – review & editing. **Seung Jae Lee:** Data curation, Investigation, Writing – original draft. **Dong Yun Lee:** Supervision, Conceptualization, Methodology, Visualization, Formal analysis, Investigation, Writing – original draft, Writing – review & editing, Project administration, Funding acquisition.

Declaration of competing interest

The authors declare no known competing financial interest.

Acknowledgements

Appendix A. Supplementary data

Supplementary data to this article can be found online at https://doi.org/10.1016/j.bioactmat.2021.06.026.

References

[1] M.E. Davis, Glioblastoma: overview of disease and treatment, Clin. J. Oncol. Nurs. 20 (5 Suppl) (2016) S2–S8.

[2] A. Omuro, L.M. DeAngelis, Glioblastoma and other malignant gliomas A clinical review, JAMA, J. Am. Med. Assoc. 310 (17) (2013) 1842–1850.

[3] O. van Tellingen, B. Yetkin-Arik, M.C. de Gooijer, P. Wesseling, T. Wurdinger, H. E. de Vries, Overcoming the blood-brain tumor barrier for effective glioblastoma treatment, Drug Resist. Updates 19 (2015) 1–12.

[4] Q.T. Ostrom, H. Gittleman, J. Fulop, M. Liu, R. Blanda, C. Kromer, Y. Wolinsky, C. Kruchko, J.S. Barnholtz-Sloan, CBTRUS statistical report: primary brain and central nervous system tumors diagnosed in the United States in 2008-2012, Neuro Oncol 17 Suppl 4 (2015) iv1–iv62.

[5] J.B. Vines, J.H. Yoon, N.E. Ryu, D.J. Lim, H. Park, Gold nanoparticles for photothermal cancer therapy, Front Chem 7 (2019) 167.

[6] X. Huang, M.A. El-Sayed, Gold nanoparticles: optical properties and implementations in cancer diagnosis and photothermal therapy, J. Adv. Res. 1 (1) (2010) 13–28.

[7] J.P. Minton, C.D. Moody, J.R. Dearman, W.B. McKnight, A.S. Ketcham, An evaluation of the physical response of malignant tumor implants to pulsed laser radiation, Surg. Gynecol. Obstet. 121 (1965) 538–544.

[8] A.B. Etame, C.A. Smith, W.C.W. Chan, J.T. Rutka, Design and potential application of PEGylated gold nanoparticles with size-dependent permeation through brain microvasculature, Nanomed-Nanotechnol 7 (6) (2011) 992–1000.

[9] J. Frigell, I. Garcia, V. Gomez-Vallejo, J. Llop, S. Penades, 68Ga-labeled gold glyconanoparticles for exploring blood-brain barrier permeability: preparation, biodistribution studies, and improved brain uptake via neuropeptide conjugation, J. Am. Chem. Soc. 136 (1) (2014) 449–457.

[10] H. Maeda, J. Wu, T. Sawa, Y. Matsumura, K. Hori, Tumor vascular permeability and the EPR effect in macromolecular therapeutics: a review, J. Contr. Release 65 (1–2) (2000) 271–284.

[11] S.A. Jensen, E.S. Day, C.H. Ko, L.A. Hurley, J.P. Luciano, F.M. Kouri, T.J. Merkel, A.J. Luthi, P.C. Patel, J.I. Cutler, W.L. Daniel, A.W. Scott, M.W. Rotz, T.J. Meade, D.A. Giljohann, C.A. Mirkin, A.H. Stegh, Spherical nucleic acid nanoparticle conjugates as an RNAi-based therapy for glioblastoma, Sci. Transl. Med. 5 (209) (2013).

[12] S.K. Golombek, J.N. May, B. Theek, L. Appold, N. Drude, F. Kiessling, T. Lammers, Tumor targeting via EPR: strategies to enhance patient responses, Adv. Drug Deliv. Rev. 130 (2018) 17–38.

[13] A. Banerjee, J. Qi, R. Gogoi, J. Wong, S. Mitragotri, Role of nanoparticle size, shape and surface chemistry in oral drug delivery, J. Contr. Release 238 (2016) 176–185.

[14] F. Araujo, J. das Neves, J.P. Martins, P.L. Granja, H.A. Santos, B. Sarmento, Functionalized materials for multistage platforms in the oral delivery of biopharmaceuticals, Prog. Mater. Sci. 89 (2017) 306–344.

[15] K. Moodley, V. Pillay, Y.E. Choonara, L.C. du Toit, V.M.K. Ndesendo, P. Kumar, S. Cooppan, P. Bawa, Oral drug delivery systems comprising altered geometric configurations for controlled drug delivery, Int. J. Mol. Sci. 13 (1) (2012) 18–43.

[16] G. Mittal, M.N. Kumar, Impact of polymeric nanoparticles on oral pharmacokinetics: a dose-dependent case study with estradiol, J. Pharmaceut. Sci. 98 (10) (2009) 3730–3734.

[17] L.M. Ensign, R. Cone, J. Hanes, Oral drug delivery with polymeric nanoparticles: the gastrointestinal mucus barriers, Adv. Drug Deliv. Rev. 64 (6) (2012) 557–570.

[18] B. Homayun, X. Lin, H.J. Choi, Challenges and recent progress in oral drug delivery systems for biopharmaceuticals, Pharmaceutics 11 (3) (2019).

[19] J. Fallingborg, Intraluminal pH of the human gastrointestinal tract, Dan. Med. Bull. 46 (3) (1999) 183–196.

[20] R. Wang, S.K. Both, M. Geven, L. Calucci, C. Forte, P.J. Dijkstra, M. Karperien, Kinetically stable metal ligand charge transfer complexes as crosslinks in nanogels/hydrogels: physical properties and cytotoxicity, Acta Biomater. 26 (2015) 136–144.

[21] C.A. Smith, C.A. Simpson, G. Kim, C.J. Carter, D.L. Feldheim, Gastrointestinal bioavailability of 2.0 nm diameter gold nanoparticles, ACS Nano 7 (5) (2013) 3991–3996.

[22] B. Ji, J. Maeda, M. Higuchi, K. Inoue, H. Akita, H. Harashima, T. Suhara, Pharmacokinetics and brain uptake of lactoferrin in rats, Life Sci. 78 (8) (2006) 851–855.

[23] S. Kumari, S.M. Ahsan, J.M. Kumar, A.K. Kondapi, N.M. Rao, Overcoming blood brain barrier with a dual purpose Temozolomide loaded Lactoferrin nanoparticles for combating glioma (SERP-17-12433), Sci. Rep. 7 (1) (2017) 6602.

[24] C. Guo, J.L. Yarger, Characterizing gold nanoparticles by NMR spectroscopy, Magn. Reson. Chem. 56 (11) (2018) 1074–1082.

[25] Z. Wu, C. Gayathri, R.R. Gil, R. Jin, Probing the structure and charge state of glutathione-capped Au25(SG)18 clusters by NMR and mass spectrometry, J. Am. Chem. Soc. 131 (18) (2009) 6535–6542.

[26] O.A. Wong, C.L. Heinecke, A.R. Simone, R.L. Whetten, C.J. Ackerson, Ligand symmetry-equivalence on thiolate protected gold nanoclusters determined by NMR spectroscopy, Nanoscale 4 (14) (2012) 4099–4102.

[27] A. Kolate, D. Baradia, S. Patil, I. Vhora, G. Kore, A. Misra, Peg - a versatile conjugating ligand for drugs and drug delivery systems, J. Contr. Release 192 (2014) 67–81.

[28] S.D. Huo, S.B. Jin, X.W. Ma, X.D. Xue, K.N. Yang, A. Kumar, P.C. Wang, J.C. Zhang, Z.B. Hu, X.J. Liang, Ultrasmall gold nanoparticles as carriers for nucleus-based gene therapy due to size-dependent nuclear entry, ACS Nano 8 (6) (2014) 5852–5862.

[29] J.Y. Chen, D.L. Wang, J.F. Xi, L. Au, A. Siekkinen, A. Warsen, Z.Y. Li, H. Zhang, Y. N. Xia, X.D. Li, Immuno gold nanocages with tailored optical properties for targeted photothermal destruction of cancer cells, Nano Lett. 7 (5) (2007) 1318–1322.

[30] Y.H. Wang, S.P. Chen, A.H. Liao, Y.C. Yang, C.R. Lee, C.H. Wu, P.C. Wu, T.M. Liu, C.R.C. Wang, P.C. Li, Synergistic delivery of gold nanorods using multifunctional microbubbles for enhanced plasmonic photothermal therapy, Sci Rep-Uk 4 (2014).

[31] J.M. Harris, R.B. Chess, Effect of pegylation on pharmaceuticals, Nat. Rev. Drug Discov. 2 (3) (2003) 214–221.

[32] Y. Nojima, Y. Suzuki, K. Yoshida, F. Abe, T. Shiga, T. Takeuchi, A. Sugiyama, H. Shimizu, A. Sato, Lactoferrin conjugated with 40-kDa branched poly(ethylene glycol) has an improved circulating half-life, Pharm Res-Dord 26 (9) (2009) 2125–2132.

[33] S.A. Lopez, E.B. Nonnecke, B.L. Lonnerdal, The lactoferrin receptor is differentially expressed across several human epithelial cell types, Faseb. J. 26 (2012).

[34] R.B. van Breemen, Y. Li, Caco-2 cell permeability assays to measure drug absorption, Expet Opin. Drug Metabol. Toxicol. 1 (2) (2005) 175–185.

[35] P. Artursson, C. Magnusson, Epithelial transport of drugs in cell-culture .2. Effect of extracellular calcium-concentration on the paracellular transport of drugs of

[36] different lipophilicities across monolayers of intestinal epithelial (Caco-2) cells, J. Pharmaceut. Sci. 79 (7) (1990) 595–600.

[36] P. Artursson, Epithelial transport of drugs in cell-culture .1. A model for studying the passive diffusion of drugs over intestinal absorptive (Caco-2) cells, J. Pharmaceut. Sci. 79 (6) (1990) 476–482.

[37] Y.A. Suzuki, V. Lopez, B. Lonnerdal, Mammalian lactoferrin receptors: structure and function, Cell. Mol. Life Sci. 62 (22) (2005) 2560–2575.

[38] Y.A. Suzuki, B. Lonnerdal, Characterization of mammalian receptors for lactoferrin, Biochem. Cell. Biol. 80 (1) (2002) 75–80.

[39] T.E. Park, N. Mustafaoglu, A. Herland, R. Hasselkus, R. Mannix, E.A. FitzGerald, R. Prantil-Baun, A. Watters, O. Henry, M. Benz, H. Sanchez, H.J. McCrea, L. C. Goumnerova, H.W. Song, S.P. Palecek, E. Shusta, D.E. Ingber, Hypoxia-enhanced Blood-Brain Barrier Chip recapitulates human barrier function and shuttling of drugs and antibodies, Nat. Commun. 10 (1) (2019) 2621.

[40] M.E. Oraiopoulou, E. Tzamali, G. Tzedakis, A. Vakis, J. Papamatheakis, V. Sakkalis, In Vitro/In Silico Study on the Role of Doubling Time Heterogeneity among Primary Glioblastoma Cell Lines, BioMed Research International 2017 (2017). Article ID 8569328, 12 pages, https://doi.org/10.1155/2017/8569328So.

[41] M.D. Donovan, G.L. Flynn, G.L. Amidon, Absorption of polyethylene glycol-600 through polyethylene glycol-2000 - the molecular-weight dependence of gastrointestinal and nasal absorption, Pharm Res-Dord 7 (8) (1990) 863–868.

[42] A. Alalaiwe, G. Roberts, P. Carpinone, J. Munson, S. Roberts, Influence of PEG coating on the oral bioavailability of gold nanoparticles in rats, Drug Deliv. 24 (1) (2017) 591–598.

[43] E. Belykh, K.V. Shaffer, C.Q. Lin, V.A. Byvaltsev, M.C. Preul, L.K. Chen, Blood-brain barrier, blood-brain tumor barrier, and fluorescence-guided neurosurgical oncology: delivering optical labels to brain tumors, Front Oncol 10 (2020).

[44] S.W. Schneider, T. Ludwig, L. Tatenhorst, S. Braune, H. Oberleithner, V. Senner, W. Paulus, Glioblastoma cells release factors that disrupt blood-brain barrier features, Acta Neuropathol. 107 (3) (2004) 272–276.

[45] H. Wolburg, K. Wolburg-Buchholz, J. Kraus, G. Rascher-Eggstein, S. Liebner, S. Hamm, F. Duffner, E.H. Grote, W. Risau, B. Engelhardt, Localization of claudin-3 in tight junctions of the blood-brain barrier is selectively lost during experimental autoimmune encephalomyelitis and human glioblastoma multiforme, Acta Neuropathol. 105 (6) (2003) 586–592.

[46] T.A. Martin, W.G. Jiang, Loss of tight junction barrier function and its role in cancer metastasis, Bba-Biomembranes 1788 (4) (2009) 872–891.

[47] W.H. De Jong, W.I. Hagens, P. Krystek, M.C. Burger, A.J.A.M. Sips, R.E. Geertsma, Particle size-dependent organ distribution of gold nanoparticles after intravenous administration, Biomaterials 29 (12) (2008) 1912–1919.

[48] G. von Maltzahn, J.H. Park, A. Agrawal, N.K. Bandaru, S.K. Das, M.J. Sailor, S. N. Bhatia, Computationally guided photothermal tumor therapy using long-circulating gold nanorod antennas, Canc. Res. 69 (9) (2009) 3892–3900.

[49] M. Semmler-Behnke, W.G. Kreyling, J. Lipka, S. Fertsch, A. Wenk, S. Takenaka, G. Schmid, W. Brandau, Biodistribution of 1.4-and 18-nm gold particles in rats, Small 4 (12) (2008) 2108–2111.

[50] Y.S. Chen, Y.C. Hung, I. Liau, G.S. Huang, Assessment of the in vivo toxicity of gold nanoparticles, Nanoscale Res Lett 4 (8) (2009) 858–864.

[51] S.K. Balasubramanian, J. Jittiwat, J. Manikandan, C.N. Ong, L.E. Yu, W.Y. Ong, Biodistribution of gold nanoparticles and gene expression changes in the liver and spleen after intravenous administration in rats, Biomaterials 31 (8) (2010) 2034–2042.

[52] A.L. Bailly, F. Correard, A. Popov, G. Tselikov, F. Chaspoul, R. Appay, A. Al-Kattan, A.V. Kabashin, D. Braguer, M.A. Esteve, In vivo evaluation of safety, biodistribution and pharmacokinetics of laser-synthesized gold nanoparticles, Sci. Rep. 9 (1) (2019) 12890.

[53] Y.C. Dong, M. Hajfathalian, P.S.N. Maidment, J.C. Hsu, P.C. Naha, S. Si-Mohamed, M. Breuilly, J. Kim, P. Chhour, P. Douek, H.I. Litt, D.P. Cormode, Effect of gold nanoparticle size on their properties as contrast agents for computed tomography, Sci Rep-Uk 9 (2019).

[54] T. Watanabe, K. Chibana, T. Shiobara, R. Tei, R. Koike, Y. Nakamura, R. Arai, Y. Horigane, Y. Shimizu, A. Takemasa, T. Fukuda, S.E. Wenzel, Y. Ishii, Expression of intelectin-1 in bronchial epithelial cells of asthma is correlated with T-helper 2 (Type-2) related parameters and its function, Allergy Asthma Clin. Immunol. 13 (2017).

[55] B.D. Kurmi, V. Gajbhiye, J. Kayat, N.K. Jain, Lactoferrin-conjugated dendritic nanoconstructs for lung targeting of methotrexate, J. Pharmaceut. Sci. 100 (6) (2011) 2311–2320.

[56] P.P. Ward, M. Mendoza-Meneses, G.A. Cunningham, O.M. Conneely, Iron status in mice carrying a targeted disruption of lactoferrin, Mol. Cell Biol. 23 (1) (2003) 178–185.

[57] S. Tsuji, J. Uehori, M. Matsumoto, Y. Suzuki, A. Matsuhisa, K. Toyoshima, T. Seya, Human intelectin is a novel soluble lectin that recognizes galactofuranose in carbohydrate chains of bacterial cell wall, J. Biol. Chem. 276 (26) (2001) 23456–23463.